ICJK
Journal of Materials Durability and Engineering
http://dx.doi.org/10.62762/JMDE.2025.161346

RESEARCH ARTICLE

Check for updates

Effect of Scanning Power on Electrochemical Corrosion Properties of AlCoCrFeNi High Entropy Alloy Coating Melted by Extremely High-speed Laser Cladding

Hao Zhang[1,*], Mengying Qiao[1], Xiujie Yue[1] and Miaomiao Xin[1]

[1] Research Institute for Reliability Manufacturing of Intelligent High-End Equipment, Qilu Institute of Technology, Jinan 250200, China

Abstract

High-entropy alloy (HEA) coatings have become a candidate for corrosion protection of marine engineering equipment in harsh service environments. In this paper, the effect of laser scanning power on the microstructure and electrochemical corrosion resistance of HEA coating prepared by Extremely High-speed Laser Cladding (EHLC) was investigated. The coating was prepared by EHLC technology. The microstructure of the coating was characterized by XRD and SEM. The corrosion resistance of the coating in 3.5% NaCl solution was investigated by electrochemical measurement. The results show that: With the increase of scanning power, the sputtered particles of the coating decreased, but the surface roughness increased. The coating was composed of FCC+BCC phases; the σ phase appeared at 200W and disappeared at 250W, and the lattice expanded with the increase of scanning power. The corrosion resistance test showed that the corrosion resistance of the coating at 200W was the best ($E_{corr} = -0.69\,V$, $I_{corr} = 6.29 \times 10^{-6}\,A/cm^2$, $R_p = 5631.67\,\Omega \cdot cm^2$ and $R_{ct} = 3030.00\,\Omega \cdot cm^2$, respectively), followed by 250W and 150W. The microstructure uniformity of the coating can be optimized by moderately increasing the scanning power (200W), and the corrosion resistance of the coating can be significantly improved, which provides a process guide for the preparation of protective coatings for offshore engineering equipment.

Keywords: extremely high-speed laser cladding, high entropy alloy coatings, scanning power, microstructure, corrosion resistance.

1 Introduction

With the development of marine resources in deep water, far sea, and polar regions, marine engineering equipment (such as ship propellers, key components of drilling platforms, seawater pump valves, etc.) is facing an increasingly harsh service environment [1]. These components suffer from corrosion in high salinity and high humidity marine environments for a long time, which leads

Submitted: 26 November 2025
Revised: 26 December 2025
Accepted: 06 January 2026
Published: 12 August 2026

Vol. 1, **No.** 1, 2026.
10.62762/JMDE.2025.161346

***Corresponding author:**
✉ Hao Zhang
zh15695603896@163.com

Citation
Zhang, H., Qiao, M., Yue, X., & Xin, M. (2026). Effect of Scanning Power on Electrochemical Corrosion Properties of AlCoCrFeNi High Entropy Alloy Coating Melted by Extremely High-speed Laser Cladding. *Journal of Materials Durability and Engineering*, 1(1), 23–34.

to premature failure of materials across a range of metallic structural systems, seriously threatening the operation safety of equipment and causing huge economic losses [2–4]. Therefore, the development of advanced surface protection technology with excellent corrosion resistance has great strategic requirements for improving the service life and reliability of offshore engineering equipment.

Among many protective materials, HEAs break the design concept of traditional alloys dominated by one or two elements, and are composed of five or more elements mixed in nearly equal atomic ratios [6]. Its unique "high entropy effect", "hysteresis diffusion effect", and "lattice distortion effect" make it tend to form a simple solid solution phase structure and show extremely high thermodynamic stability and chemical stability [6]. The results show that a dense oxide film with strong passivation ability can be easily formed on the surface of a high entropy alloy by adjusting the composition reasonably [8, 42]. Wang et al. [9] found that increasing Al content progressively promotes the transition from FCC to BCC phase in AlxCoCrFeNi high-entropy alloys, and the resulting Al-enriched passive film significantly enhances the electrochemical stability and corrosion resistance of the alloy in chloride environments. In addition, the microstructure of the alloy also has a decisive effect on the corrosion behavior. Single-phase solid solution structures generally have a more uniform electrochemical activity than multiphase structures, reducing the risk of microgalvanic corrosion. Wang et al. [10] found that the addition of appropriate copper optimized the microstructure, making the AlCrFeNiCu alloy's passivation film of the alloy is more stable, thus obtaining the best corrosion resistance. It can be seen that the preparation of HEA coating can endow it with electrochemical corrosion resistance far exceeding that of traditional alloys, and become a candidate material with great potential in the field of marine equipment surface protection [5, 11].

At present, Laser-based surface modification techniques, including laser cladding, have gained wide adoption in the preparation of protective coatings due to their advantages of controllable heat input, robust metallurgical bonding with the substrate, and broad material adaptability, as well as demonstrated effectiveness in enhancing corrosion and erosion resistance of metallic components [7, 12]. Wu and Lu [13] prepared $Al_{0.7}FeCoCrNiCu_X$ high entropy alloy coatings on a light alloy substrate by laser cladding and demonstrated that the coating exhibits excellent corrosion resistance in simulated marine environments. However, conventional laser cladding processes typically employ low scan speeds (typically 5-20 mm/s) and long interaction times between the laser beam and the powder material, resulting in high energy injection densities [14]. This inevitably leads to a series of problems: First, the "dilution effect" of matrix elements on coating elements is significant [15]. Too high a dilution rate will dilute the design composition of the cladding layer, making it deviate from the preset alloy system, thus weakening the special functional properties, such as wear resistance, corrosion resistance, or high temperature resistance that the coating should have. Zhang et al. [16] found that compared with normal laser cladding, high-speed laser cladding significantly reduces heat input and dilution rate, thereby suppressing the formation of coarse microstructures and improving the overall quality of CoCrFeMnNi high-entropy alloy coatings. Second, long-term heat action will aggravate the extent of the heat-affected zone and grain coarsening [17]. Li et al. [18] found that multiple laser remelting treatments progressively refined the microstructure of $Fe_{0.5}CoCrNi_{1.5}Nb_{0.68}Mo_{0.3}$ high-entropy alloy coatings, reduced elemental segregation accumulated during solidification, and substantially improved corrosion resistance in aggressive environments. Moreover, high heat input leads to a relatively slow cooling rate of the molten pool, coating structure often grows into coarse dendrite, and easy to produce element segregation and porosity, cracks, and other defects [19, 21]. Among these, crack formation in laser cladding is particularly sensitive to process parameters such as heat input and pulse characteristics [21]. These microstructural defects serve as preferential channels for corrosive medium penetration, thus seriously deteriorating the electrochemical corrosion resistance of the coating [20]. Sun et al. [22] found that the slow cooling process of traditional laser cladding provides sufficient growth time for grains, which promotes the formation of coarse columnar or equiaxed dendrite structures inside the coating. Comparative studies on chromium-rich stainless steel coatings further confirmed that EHLC-prepared coatings exhibit significantly finer microstructures and superior corrosion resistance relative to conventionally cladded counterparts [35].

In recent years, the EHLC has emerged as a breakthrough surface modification technology. Unlike conventional laser cladding, EHLC technology achieves extremely rapid heating and cooling processes (cooling rates up to 10^5–10^6 K/s) by increasing the laser scanning speed (up to 50–200 m/s) so that the powder melts completely in the air before entering the melt pool and is subsequently sprayed onto the substrate surface in the form of droplets [23]. This unique process characteristic makes EHLC a promising platform for preparing high-performance HEA composite coatings with superior wear and corrosion resistance [24]. This process characteristic gives the coatings prepared by EHLC unique advantages: extremely low heat input significantly reduces the heat affected zone of the substrate, almost eliminates element dilution, and maintains the compositional stability of the high entropy alloy coating [25, 26]; At the same time, the ultra-high cooling rate promotes the formation of ultra-fine grain or even nanocrystalline structure, significantly reduces the grain boundary energy, and effectively inhibits the precipitation of harmful second phases, which is expected to greatly improve the electrochemical corrosion resistance of the coating [27, 28].

Although the EHLC process has shown great potential in the preparation of high-performance coatings, the influence mechanism of process parameters on coating quality, especially on corrosion resistance, needs to be further explored. During the cladding process, scanning power is a key parameter to determine energy input, molten pool morphology, and solidification behavior. Too low power will lead to insufficient powder melting, coating non-fusion defects, damage its integrity [17, 28, 29]; too high power can ensure the cladding efficiency, but may cause excessive melting of the matrix, resulting in increased dilution rate, and even cause grain coarsening or element burning due to overheating, thus affecting the stability of the passivation film coating [30]. At present, there is still a lack of systematic research on how laser scanning power regulates the microstructure evolution of EHLC HEA coatings and then affects their electrochemical corrosion behavior in the marine environment.

In view of this, AlCoCrFeNi HEA coating was prepared by EHLC technology, and the influence of laser scanning power on microstructure, element distribution, and electrochemical corrosion performance of the coating was systematically studied. The purpose is to provide a theoretical basis and process guidance for the development of corrosion-resistant HEA coatings for high-performance offshore engineering equipment.

2 Preparation and Characterization of Experimental Coatings

2.1 Material Preparation

The base material is commercial 5083 aluminum alloy with a specification of $50\,\mathrm{mm} \times 40\,\mathrm{mm} \times 3\,\mathrm{mm}$. AlCoCrFeNi HEA spherical powder was supplied by Suzhou Haichuan Rare Metal Products Co., Ltd.; the particle size of the powder is 1–$25\,\mu\mathrm{m}$, and the morphology and chemical composition are shown in Figure 1 and Table 1.

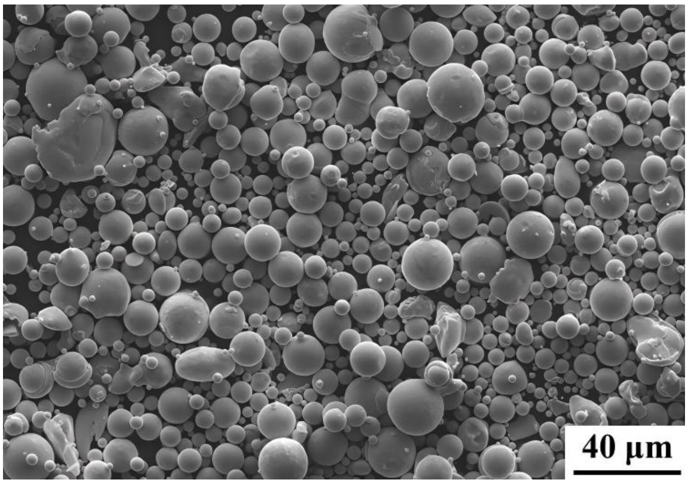

Figure 1. High entropy alloy composite coating AlCoCrFeNi powder particles.

The optimum parameters of EHLC were determined as follows: laser power: $150\,\mathrm{W}$, $200\,\mathrm{W}$, and $250\,\mathrm{W}$, scanning rate: $1000\,\mathrm{mm/s}$, and scanning interval: $0.05\,\mathrm{mm}$. A high entropy alloy coating was prepared on the alloy substrate by using the EOS M290 equipment.

2.2 Before the Coating Preparation Experiment

The surface of the plate was polished by sandpaper to remove the oxide film on the surface and make the surface of the plate smooth; then, the aluminum block was placed in 75% absolute ethanol for ultrasonic cleaning for $30\,\mathrm{min}$, and dried for later use. HEA powder is added into an 8% polyvinyl alcohol solution, and mechanically stirred for $30\,\mathrm{min}$ to prepare HEA powder slurry; then, the slurry is uniformly sprayed on the surface of a pretreated aluminum alloy test block in a spraying manner, and the spraying thickness is controlled to be $0.3\,\mathrm{mm}$ to $0.5\,\mathrm{mm}$; and then, the sprayed preset test block is put into a vacuum drying oven, and dried at $50\,^{\circ}\mathrm{C}$ for about $30\,\mathrm{min}$. Finally, after the preset layer has solidified, place the specimen with the preset coating into the EOS M290 equipment for processing. In order to avoid

Table 1. Chemical composition of the coatings.

Elemental	Al	Cr	Fe	Co	Ni
Atomic(%)	24.588	19.053	19.080	18.760	18.519

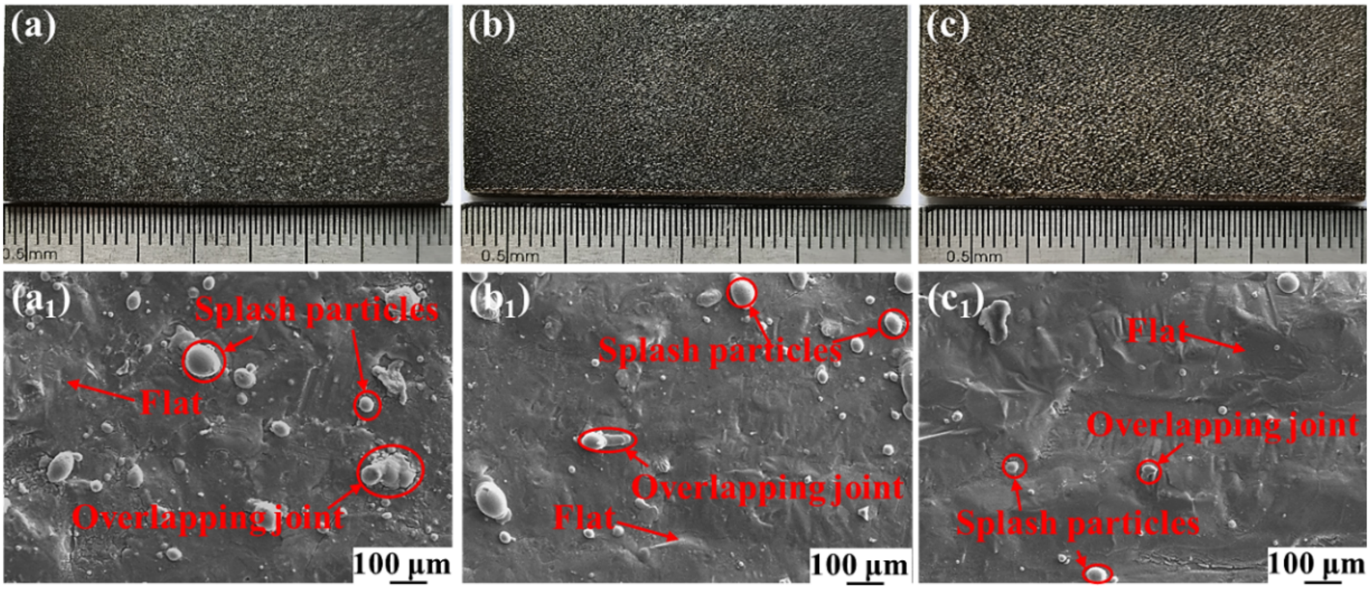

Figure 2. Surface morphology of the coatings (a) (a_1) 150 W; (b) (b_1) 200 W; (c) (c_1) 250 W.

the coating cracking caused by uneven thermal stress, the substrate should be preheated at 80 °C for 10 min before EHLC processing.

2.3 Performance and Characterization

2.3.1 Electrochemical Corrosion Performance

The Shanghai Chenhua CHI600E electrochemical workstation was used, and the three-electrode test system consisting of 3.5% NaCl solution as electrolyte, a Pt electrode of 20 mm×20 mm×1 mm as counter electrode, a saturated calomel electrode as reference electrode, and a working electrode as test sample was used to conduct electrochemical tests on the coating surface (test area: 100 mm^2) at room temperature.

2.3.2 Characterization of Coating Structure

First, the coating test sample is prepared by using an electric spark wire cutting machine, and then the coating sample is ground and polished; finally, the treated coating sample is placed in alcohol for ultrasonic cleaning to remove contaminants on the coating test surface. X-ray diffraction (XRD) phase analysis of the coating surface was performed using a Bruker D8 multi-purpose powder diffractometer. Specific conditions were as follows: X-ray source: Copper target, Scanning mode: Continuous scanning, Scanning speed: 5 °/min, Scanning range: 20°–90°. An OLS50-CB laser confocal scanning microscope (LCSM) was used to characterize and analyze the macro-morphology of the coating. A Hitachi SU8100 field emission scanning electron microscope (SEM) was used to characterize the coating. Secondary electron imaging mode and X-ray energy dispersive spectrometer (EDS) were used to analyze the morphology, structure, and element distribution of the coating.

3 Results Discussion and Analysis

3.1 Influence of Scan Power on Coat Microstructure

Figure 2 shows the surface morphology of the coating under different scanning powers. Figure 2(a–c) shows the macro-morphology of the coating surface, and the coating surface prepared by EHLC does not have obvious macro-surface defects such as cracks and pores. At the same time, no machining trace caused by traditional LC machining was observed. The overall coating is uniform and flat. Figure 2(a_1–c_1) shows the SEM morphology of the coating surface. It is found that the coating surface is intact without micro-cracks and pores, and there are different degrees of sputtered particles, flat areas, and particle overlapping areas on the coating surface. With the increase of scanning power, the sputtered particles and the overlapping area of particles in the coating obviously decrease. This phenomenon can be explained by the laser input energy equation as follows [31]:

$$E = \frac{P}{S \cdot T \cdot D} \tag{1}$$

where E, laser input energy $(\mathrm{J/mm^3})$; P, scanning power (W); S, scanning rate $(\mathrm{mm/s})$; T, coating thickness (mm); D, scanning spacing (mm). There is a close relationship between the size of E and process parameters. It can be seen that with increasing scan power, the laser energy input into the coating increases significantly, so that the coating particles are melted more thoroughly, and the occurrence of sputtered particles and particle lapping on the surface of the coating is reduced.

Figure 3 shows the surface LCSM micrographs of the coating under different scanning powers. The color change from blue to red in the legend indicates a transition in coating depth from "pit" to "bump." Table 2 shows the relevant parameters of coating surface quality. It can be seen from Figure 3 that the overall morphology of the coating surface is relatively flat, and there are no significant pits or protrusions. The overall quality of the coating is relatively good. It can be seen from Table 2 that S_a, S_q, S_p, and S_z of the coating all show an increasing trend with the increase of scanning power. When the scanning power is 250 W, the surface undulation of the coating is the largest, which fully indicates that the scanning power has a significant effect on the surface quality of the coating.

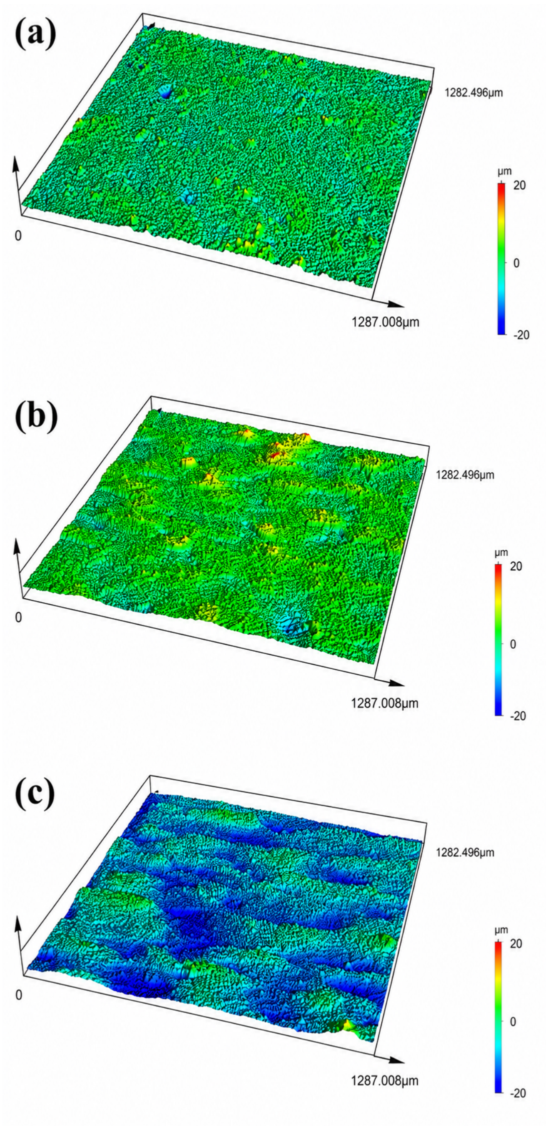

Figure 3. Microscopic morphology image of the coating's surface by LCSM (a) 150 W; (b) 200 W; (c) 250 W.

Table 2. Surface quality data of the coatings.

Scanning Power	S_q (μm)	S_p (μm)	S_z (μm)	S_a (μm)
150 W	4.80	59.29	99.46	3.53
200 W	8.78	64.78	134.31	6.80
250 W	10.13	91.55	138.35	8.00

3.2 Influence of Scan Power on Coat Microstructure

Figure 4 shows XRD spectra of coatings at different scanning powers. The coating structure consists of BCC and FCC. When the scanning power is 150 W, the σ phase diffraction peaks at $2\theta = 33.64°$, $36.23°$ and $75.87°$ do not appear; when the scanning power is 200 W, the σ phase diffraction peaks at $2\theta = 33.64°$, $36.23°$ and $75.87°$ appear; and when the scanning power increases to 250 W, the σ phase diffraction peaks at $2\theta = 33.64°$, $36.23°$, and $75.87°$ all disappear. It shows that when the scanning power increases from 150 W to 200 W, the thermal energy in the coating promotes the diffusion of aluminum atoms from the aluminum-poor layer, and other atoms (Cr, Fe, etc.) migrate to compensate for the resulting

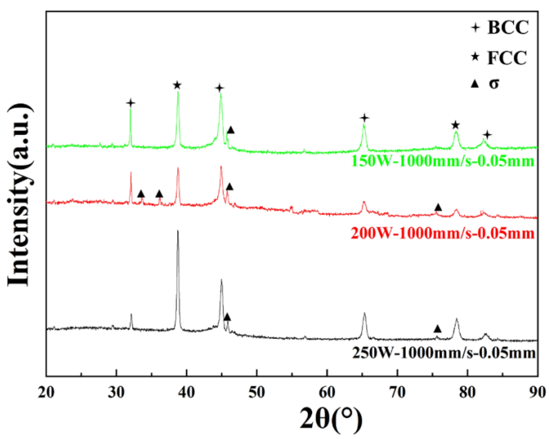

Figure 4. XRD patterns of the coatings.

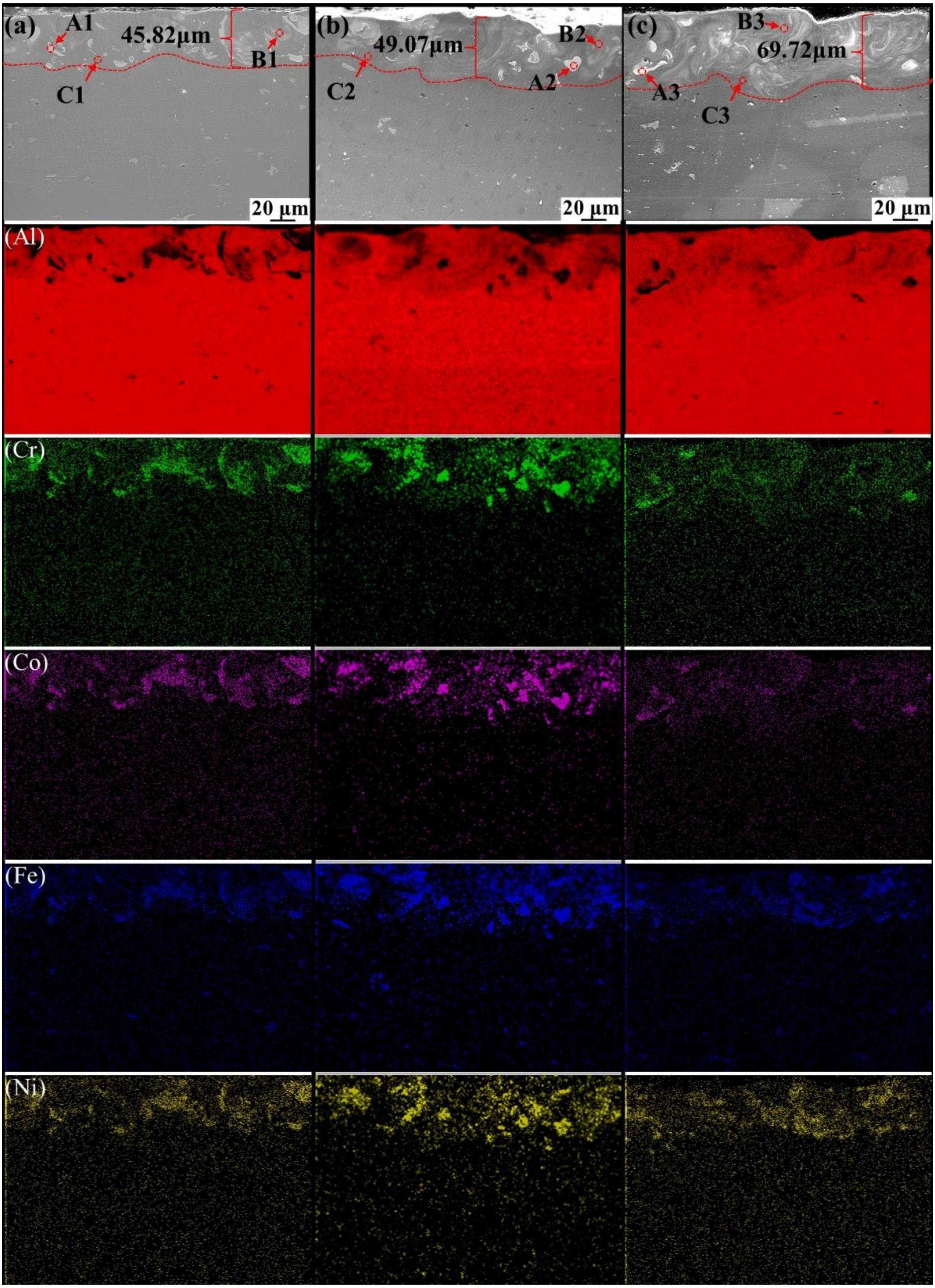

Figure 5. Cross-sectional SEM morphology and EDS element distribution morphology of the coatings (a) 150 W; (b) 200 W; (c) 250 W.

vacancies, leading to the formation of σ phase in the aluminum-poor region [34]. With the increase of scanning power to 250 W, the thermal energy in the coating increases, the melting time of particles in the coating decreases, the diffusion and migration of aluminum atoms in the aluminum-poor region of the coating are suppressed, and the diffraction peaks of the σ phase at $2\theta = 33.64^\circ$ and 36.23° disappear. In addition, with the increase of scanning power, the diffraction peak of the phase in the coating shifted slightly to the left, that is, shifted to the small-angle direction. This shift is due to lattice expansion effects induced by increased laser energy input, and its core mechanism involves increased atomic vibration, increased average atomic spacing, and increased lattice constant [33]. Cui et al. [34] confirmed this view in their study of FeCoCrNiMnAl coatings.

Figure 5 shows the SEM morphology of the cross-section of the coating and the EDS scanning results of the cross-section under different scanning powers. As can be seen from the figure, no coating defects such as microcracks and pores are found on the cross section of the coating prepared by EHLC process, and the coating quality is excellent. In addition, that thickness of the coat is between $45.82\,\mu$m and $69.72\,\mu$m, and the thickness of the coating is in a positive correlation with the scan power. The coated area can be divided into three zones (off-white (A), light gray (B), and gray (C)) based on the color of the tissue in the composite coated area (above the red dotted line). EDS analysis shows that Cr, Co, Fe, and Ni are enriched obviously in A region, and Al is almost absent in A region, while Al, Cr, Co, Fe, and Ni are distributed evenly in B region, and Al is dominant in C region. With the increase of the scanning power, the area A in the coating structure decreases and the area B increases, indicating that elemental segregation is suppressed and the coating microstructure becomes more homogeneous. This observation is consistent with findings in comparable HEA coating systems, where variations in energy input—whether through process type or parameter adjustment—have been shown to govern the extent of elemental enrichment zones and microstructural uniformity [32].

For the AlCoCrFeNi alloy system, prior studies using thermal spray techniques have similarly reported that Cr- and Ni-enriched zones exhibit elevated hardness [36, 37], suggesting that the hardness heterogeneity observed across microstructural zones in the present EHLC coatings is an intrinsic feature of this alloy composition rather than an artifact of the deposition process. This improvement in local hardness is expected to contribute to the overall wear resistance of the composite coating. In addition, the peeling phenomena, such as cracks and the like, do not occur between each element and the aluminum alloy matrix, and the coating is tightly combined with the matrix to form excellent metallurgical bonding.

3.3 Effect of Scan Power on Electrochemical Corrosion Properties of Coatings

Figure 6 is the electrochemical spectrum of the coating in NaCl solution with a mass fraction of 3.5% under different scanning powers. From the polarization curve shown in Figure 6(a), the E_{corr}, I_{corr} and R_p of the coated surface can be obtained as shown in Table 3. The polarization curves of the alloy in the solution containing 3.5% NaCl show a significant inflection point (critical pitting potential). The results show that the surface of aluminum alloy is passivated to a certain extent; that is, a protective oxide film is formed on the surface of aluminum alloy in a certain potential range. However, the polarization curves of the coatings under different scanning powers did not show similar inflection points when the coatings were subjected to similar electrochemical tests. The results show that the electrochemical corrosion of the coating surface is mainly uniform, and there is no obvious pitting corrosion. The results show that the coating has good pitting corrosion resistance.

As can be seen from the analysis of the data in Table 3, the coatings prepared with the three different scan powers exhibited some interesting properties in the electrochemical corrosion test. In particular, the E_{corr} of these coatings is generally higher than the corrosion potential of the alloy substrate. The I_{corr} and R_p values of the coating do not show an obvious trend change with the increase in scanning power. It was further observed that the E_{corr} and R_p of the coating showed a fluctuating trend of first increasing and then decreasing with the increase of scanning power. E_{corr} from small to large order is 5083 < 150 W < 250 W < 200 W, and I_{corr} from small to large order is 200 W < 250 W < 5083 Al < 150 W. R_p from small to large order is 150 W < 5083 < 250 W < 200 W.

In conclusion, when the scanning power is set to 200 W, the coating exhibits relatively excellent corrosion resistance. Under these conditions, the E_{corr} of the coating shifted 510 mV compared with that of the alloy matrix, indicating that the stability of the coating in the electrochemical polarization reaction was significantly improved. At the same time, the

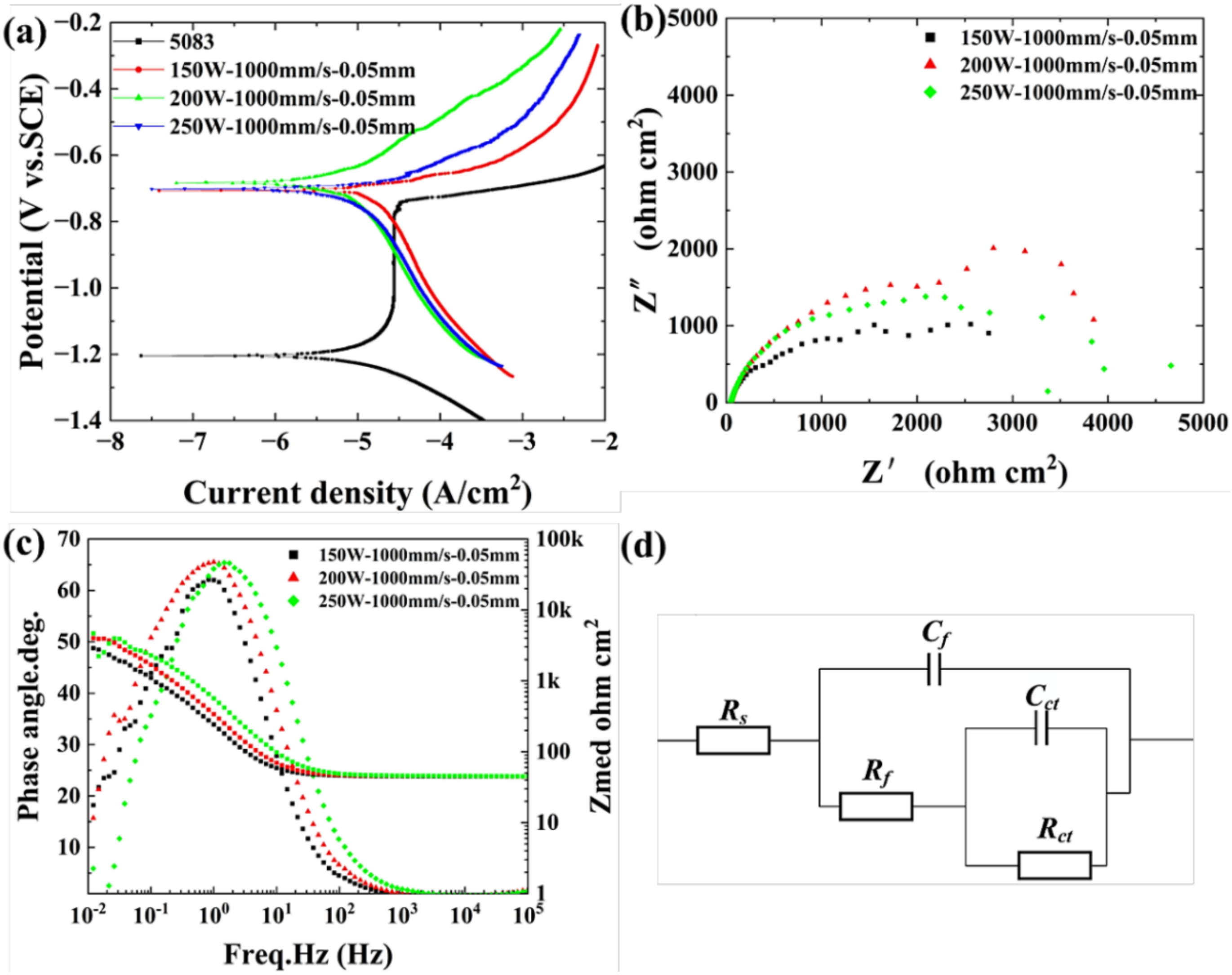

Figure 6. Electrochemical testing of the coatings in 3.5 % NaCl solution (a) Polarization curves; (b) Nyquist plots; (c) Bode plots; and (d) Fitted equivalent circuits.

Table 3. Electrochemical parameters of the coatings.

Samples	5083	150 W	200 W	250 W
E_{corr} (V)	-1.20	-0.71	-0.69	-0.70
I_{corr} (A/cm^2)	1.48×10^{-5}	2.31×10^{-5}	6.29×10^{-6}	1.19×10^{-5}
R_p (Ω·cm^2)	2672.00	2052.00	5631.67	2848.67

I_{corr} of the coating is one order of magnitude lower than that of the aluminum alloy substrate, indicating that the reaction rate of the coating in the corrosion process is significantly reduced. In addition, R_p also increased by 2.11 times, further demonstrating that the corrosion resistance of the coating was significantly enhanced. The results show that a moderate increase in scanning power can improve the corrosion resistance of the coating.

In order to obtain more corrosion information of coatings under different scanning powers, EIS tests were carried out on coatings prepared under different scanning powers. As shown in Figure 6(b), Nyquist curves usually present semicircular arcs, indicating that the corrosion behavior of coatings prepared under different scanning powers is mainly affected by the charge transfer between the coating and the electrolyte surface interface. In the process of charge transfer, the charge transfer is hindered by the inhomogeneity of the two interfaces. The capacitive arc radius reflects the coating's charge transfer resistance (R_{ct}) value in the corrosion process. The larger the capacitive arc radius, the greater the R_{ct} value and the stronger the corrosion resistance of the coating [38, 40]. EIS techniques including Nyquist analysis have been widely employed to characterize the corrosion performance of thermally deposited and laser-processed coatings across diverse alloy systems [39]. According to the Nyquist curve of coating, the order of capacitance arc radius is 200W sample with the largest radius, 250W sample with the second largest radius, and 150W sample with the smallest radius. The results show that the 200W sample has the largest R_{ct} and the best corrosion resistance, followed by the 250W sample, and the 150W sample has relatively poor corrosion resistance. This conclusion is consistent with the results obtained from the polarization curve test. I_{corr} is usually used to characterize the corrosion resistance of materials in a polarization curve test. The smaller the I_{corr} value, the better the corrosion resistance of the material [40]. Therefore, combining the Nyquist curve and polarization curve test results, it can be concluded that the corrosion resistance of the coating prepared at 200W, 250W, and 150W scanning power is the best, followed by the 250W sample, and the 150W sample is the worst.

Figure 6(c) shows the Bode plots of the coatings at different scanning powers. In the high-frequency region, $\log|Z|$ represents the magnitude of the solution's resistance. During electrochemical impedance testing, the electrolyte was uniformly a 3.5% NaCl solution, resulting in similar resistance characteristics across the three samples in the high-frequency range. However, in the low-frequency region, $\log|Z|$ more accurately reflects the resistance properties of the passivation film on the coating surface [41]. Specifically, compared to the coating prepared at $250\,\mathrm{W}$ scanning power, the coating prepared at 200 W scanning power exhibits a slightly higher $\log|Z|$ in the low-frequency region, and both are significantly higher than the $\log|Z|$ of the sample prepared at $150\,\mathrm{W}$ laser scanning power. This indicates that as the scanning power increases, the resistance of the passivation film on the coating surface is significantly enhanced. This trend aligns with the variation in R_{ct} observed in the Nyquist plot. In the mid-frequency range, the coating exhibits its maximum phase angle. The width of this frequency range reflects the stability of the passivation film during corrosion [42]. A broader frequency range indicates superior stability of the passivation film throughout the corrosion process [8, 43]. By examining the frequency range width of the stable phase angle region in the mid-frequency range across the three samples in the Bode plot, the sequence is observed as follows: the $200\,\mathrm{W}$ sample exhibits the widest frequency range, followed by the $250\,\mathrm{W}$ sample, while the $150\,\mathrm{W}$ sample has the narrowest frequency range. This sequence perfectly aligns with the order of R_{ct} magnitude in the Nyquist plot.

Table 4. Fitting parameters of the equivalent circuit model for the coatings.

Samples	150 W	200 W	250 W
R_s $(\Omega \cdot \mathrm{cm}^2)$	46.60	47.00	47.30
C_f $(\mu\mathrm{F} \cdot \mathrm{cm}^2)$	6.20×10^{-4}	4.08×10^{-4}	2.07×10^{-4}
R_f $(\Omega \cdot \mathrm{cm}^2)$	854.00	998.00	897.00
C_{ct} $(\mu\mathrm{F} \cdot \mathrm{cm}^2)$	1.75×10^{-3}	7.94×10^{-4}	3.16×10^{-4}
R_{ct} $(\Omega \cdot \mathrm{cm}^2)$	1710.00	3030.00	2480.00

The fitting circuit model of $R_s(C_f R_f(C_{ct} R_{ct}))$ is used to establish the equivalent circuit of the coating corrosion process under different scanning powers, as shown in Figure 6(d). The fitting parameter values are shown in Table 4. The analysis shows that the values of passivation resistance (R_f) and R_{ct} show a certain regularity. Specifically, both R_f and R_{ct} reach a maximum at $200\,\mathrm{W}$, decrease as the scan power increases to $250\,\mathrm{W}$, and decrease as the scan power decreases to $150\,\mathrm{W}$. This phenomenon indicates that the charge transfer resistance of the coating surface and interface is the largest when the scanning power is $200\,\mathrm{W}$, and the corrosion resistance of the coating is the best. The result is consistent with that observed in the polarization curves, Nyquist plots, and Bode plots. The results show that the corrosion resistance of coatings prepared at different scanning powers is the best at $200\,\mathrm{W}$, the second is at $250\,\mathrm{W}$, and the corrosion resistance of coatings prepared at $150\,\mathrm{W}$ is relatively poor.

4 Conclusion

(1) The AlCoCrFeNi coating prepared by the EHLC process has excellent quality without obvious microcracks and pores in cross-section. The coating thickness is positively correlated with scanning power. EDS analysis shows that the coating is mainly composed of Al, Co, Cr, Fe, and Ni elements, and there is element enrichment in the gray-white region. With the increase of scanning power, the gray-white enrichment region decreases, and the uniformity of the coating structure is improved significantly. There is no spalling crack between the coating and the substrate, forming a close metallurgical bonding.

(2) FCC phase and BCC phase are the main phases of the coating. The diffusion and migration of Al atoms in the Al-deficient region of the coating can be suppressed with increasing scanning power, resulting in the disappearance of σ phase diffraction peaks at $2\theta = 33.64°$, $36.23°$, and $75.87°$. In addition, with the increase of scanning power, the input energy of the alloy system increases, the atomic vibration intensifies, the average atomic distance enlarges, causing lattice expansion, the metal atom migration convenience improves, the phase diffraction peak shifts to the small angle direction, and the lattice constant increases.

(3) The coating exhibits predominantly uniform corrosion in a 3.5% NaCl solution, with no significant pitting corrosion, demonstrating excellent pitting resistance. The E_{corr} values for this coating are generally higher than those of the substrate. Both E_{corr} and R_p initially increase, then decrease with increasing scan power, while I_{corr} shows the opposite trend. At a scanning power of $200\,\mathrm{W}$, compared to the substrate, the coating's E_{corr} shifted positively by $510\,\mathrm{mV}$, I_{corr} decreased by one order of magnitude, R_p increased by 2.11 times, R_{ct} reached its maximum, $\log|Z|$ peaked in the low-frequency region, the phase angle exhibited the widest stable range in the mid-frequency region, and the interfacial charge migration resistance was highest, resulting in optimal corrosion resistance. At a scanning power of $150\,\mathrm{W}$, the coating exhibited the poorest corrosion resistance, followed by $250\,\mathrm{W}$. The study indicates that moderately increasing the scanning power can effectively enhance the coating's corrosion resistance.

Data Availability Statement

Data will be made available on request.

Funding

This work was supported by the Research Program of Qilu Institute of Technology, China under Grant QIT25TP032.

Conflicts of Interest

The authors declare no conflicts of interest.

AI Use Statement

The authors declare that no generative AI was used in the preparation of this manuscript.

Ethical Approval and Consent to Participate

Not applicable.

References

[1] Wu, Y., Zhao, W., & Wang, L. (2025). State of the art and current trends on the metal corrosion and protection strategies in deep sea. *Journal of Materials Science & Technology, 215*, 192-213. [CrossRef]

[2] Liang, J., Wang, W., Cao, Z., Guo, J., Sun, Z., & Hai, Y. (2024). Corrosion resistance and mechanism of high-entropy alloys: A review. *Materials and Corrosion, 75*(4), 424-432. [CrossRef]

[3] Zhang, B. B., Zhang, R. Y., Wang, Y., Wang, W., & Sand, W. (2024). Preface: Corrosion and protection in marine environment. *Journal of Central South University, 31*(10), 3349-3351. [CrossRef]

[4] Nassar, N. E. A. (2022). Corrosion in marine and offshore steel structures: Classification and overview. *International Journal of Advanced Engineering, Sciences and Applications, 3*(1), 7-11. [CrossRef]

[5] Wang, J., Wen, W., Xie, F., Wu, B., Yang, Y., Cheng, J., ... & Zhang, X. (2024). Effects of oxygen concentration on the corrosion behavior of high entropy alloy AlCoCrFeNi in simulated deep sea. *Heliyon, 10*(12). [CrossRef]

[6] Nartita, R., Ionita, D., & Demetrescu, I. (2024). A modern approach to HEAs: from structure to properties and potential applications. *Crystals, 14*(5), 451. [CrossRef]

[7] Liu, C., Tong, S., Yue, Y., Wang, H., Song, J., Li, Y., ... & Wang, Z. (2024). Laser-based fabrication of superwetting titanium alloy with enhanced corrosion and erosion-corrosion resistance. *Colloids and Surfaces A: Physicochemical and Engineering Aspects, 688*, 133648. [CrossRef]

[8] Wang, K., Zhu, Y., Wang, P. W., Li, X., Malomo, B., & Yang, L. (2024). Enhancing corrosion resistance in CoCrFeNiTa high entropy alloys via Mo addition. *Electrochimica Acta, 480*, 143951. [CrossRef]

[9] Wang, Y., Li, G., Qi, H., Zhang, W., Chen, R., Su, R., & Qu, Y. (2024). Effect of Al content on the corrosion behavior and mechanism of AlxCoCrFeNi high-entropy alloys. *Journal of Materials Research and Technology, 30*, 5977-5989. [CrossRef]

[10] Wang, J., Jiang, H., Chang, X., Zhang, L., Wang, H., Zhu, L., & Qin, S. (2023). Effect of Cu content on the microstructure and corrosion resistance of AlCrFeNi3Cux high entropy alloys. *Corrosion Science, 221*, 111313. [CrossRef]

[11] Fu, Y., Li, J., Luo, H., Du, C., & Li, X. (2021). Recent advances on environmental corrosion behavior and mechanism of high-entropy alloys. *Journal of Materials Science & Technology, 80*, 217-233. [CrossRef]

[12] Zhang, C., Huang, L., Li, S., Li, K., Lu, S., & Li, J. (2023). Improved corrosion resistance of laser melting deposited CoCrFeNi-series high-entropy alloys by Al

addition. *Corrosion Science, 225*, 111599. [CrossRef]

[13] Wu, X., & Lu, Y. (2022). Study on the corrosion resistance of laser clad Al0.7FeCoCrNiCux high-entropy alloy coating in marine environment. *Coatings*, *12*(12), 1855. [CrossRef]

[14] Tabernero, I., Lamikiz, A., Martínez, S., Ukar, E., & De Lacalle, L. L. (2012). Modelling of energy attenuation due to powder flow-laser beam interaction during laser cladding process. *Journal of materials processing technology, 212*(2), 516-522. [CrossRef]

[15] Liu, J., Bai, M., Xu, W., & Chu, T. (2025). Effect of Processing Parameters on the Microstructure and Corrosion Properties of AlCrFeCoNi High-Entropy Alloy Coatings Fabricated by Laser Cladding. *Metals, 15*(3), 231. [CrossRef]

[16] Zhang, Q., Wang, Q., Han, B., Li, M., Hu, C., & Wang, J. (2023). Comparative studies on microstructure and properties of CoCrFeMnNi high entropy alloy coatings fabricated by high-speed laser cladding and normal laser cladding. *Journal of Alloys and Compounds, 947*, 169517. [CrossRef]

[17] Zhou, L., Ma, G., Zhao, H., Mou, H., Xu, J., Wang, W., ... & Wang, H. (2024). Research status and prospect of extreme high-speed laser cladding technology. *Optics & Laser Technology, 168*, 109800. [CrossRef]

[18] Li, Y., Wang, L., Zhang, J., Liu, M., Guo, S., Liu, J., & Cao, L. (2024). Effect of multiple laser remelting on microstructure and corrosion resistance of Fe0. 5CoCrNi1. 5Nb0. 68Mo0. 3 high entropy alloy coatings. *Journal of Materials Research and Technology, 31*, 3935-3949. [CrossRef]

[19] Zhan, X., Qi, C., Gao, Z., Tian, D., & Wang, Z. (2019). The influence of heat input on microstructure and porosity during laser cladding of Invar alloy. *Optics & Laser Technology, 113*, 453-461. [CrossRef]

[20] Li, B., Zhu, H., Qiu, C., & Guo, D. (2020). Development of multi-principal-component alloy coating by laser cladding with excellent mechanical and corrosion properties. *Journal of Alloys and Compounds, 820*, 153071. [CrossRef]

[21] Zhang, Z., Zhao, Y., Chen, Y., Su, Z., Shan, J., Wu, A., ... & Tang, X. (2021). The role of the pulsed-wave laser characteristics on restraining hot cracking in laser cladding non-weldable nickel-based superalloy. *Materials & Design, 198*, 109346. [CrossRef]

[22] Sun, P., Liang, J., Ma, D., Tang, C., Wang, D., Lai, T., & Zhang, H. (2025). Microstructural evolution and corrosion behavior of Fe-Cr-B alloy coatings: A comparative study between extreme high-speed and traditional laser cladding. *Surface and Coatings Technology, 513*, 132542. [CrossRef]

[23] Liang, Y., Liao, Z. Y., Zhang, L. L., Cai, M. W., Wei, X. S., & Shen, J. (2023). A review on coatings deposited by extreme high-speed laser cladding: processes, materials, and properties. *Optics & Laser Technology, 164*, 109472. [CrossRef]

[24] Zhou, J. L., Cheng, Y. H., He, B., Wan, Y. X., Chen, H., Wang, Y. F., & Yang, J. Y. (2025). Enhancement of high-entropy alloy coatings with multi-scale TiC ceramic particles via high-speed laser cladding: Microstructure, wear and corrosion. *Applied Surface Science, 685*, 162061. [CrossRef]

[25] Chong, Z., Sun, Y., Cheng, W., Huang, L., Han, C., Ma, X., & Meng, A. (2022). Laser remelting induces grain refinement and properties enhancement in high-speed laser cladding AlCoCrFeNi high-entropy alloy coatings. *Intermetallics, 150*, 107686. [CrossRef]

[26] Meghwal, A., Pinches, S., Anupam, A., Lie, L., Munroe, P., Berndt, C. C., & Ang, A. S. M. (2023). Structure-property correlation of a CoCrFeNi medium-entropy alloy manufactured using extreme high-speed laser material deposition (EHLA). *Intermetallics, 152*, 107769. [CrossRef]

[27] Chen, S., Zhou, Y., Peng, P., Guo, S., Yang, L., & Guo, C. (2025). Wear and corrosion resistance of 304SS coating using high speed laser cladding. *International Journal of Precision Engineering and Manufacturing, 26*(6), 1527-1539. [CrossRef]

[28] Shen, F., Tao, W., Li, L., Zhou, Y., Wang, W., & Wang, S. (2020). Effect of microstructure on the corrosion resistance of coatings by extreme high speed laser cladding. *Applied Surface Science, 517*, 146085. [CrossRef]

[29] Wu, Y., Lu, K., Zhu, J., Guo, D., Yang, M., Sun, H., Wang, Z., & Hui, X. (2022). Microstructures, corrosion resistance and wear resistance of high-entropy alloys coatings with various compositions prepared by laser cladding: A review. *Coatings, 12*(7), 1023. [CrossRef]

[30] Gao, Q., Liu, H., Chen, P., Liu, X., Yang, H., & Hao, J. (2023). Multi-objective optimization for laser cladding refractory MoNbTiZr high-entropy alloy coating on Ti6Al4V. *Optics & Laser Technology, 161*, 109220. [CrossRef]

[31] Zhang, H., Qiao, M., Liu, X., Wang, Y., & Duan, J. (2025). Research on the laser melting coating process of an AlCoCrFeNi high-entropy alloy. *International Journal of Applied Ceramic Technology, 22*(2), e14937. [CrossRef]

[32] Xie, F., Zhai, C., Zhang, X., Emre, A., Zheng, H., Zhang, X., ... & Hua, X. (2025). Microstructure, dislocation and high-temperature oxidation behavior of as-cladding NiCoFeCrMo high-entropy alloy coatings: Laser cladding vs vacuum cladding. *Journal of Alloys and Compounds, 1033*, 181278. [CrossRef]

[33] Zhang, Q., Li, M., Wang, Q., Qi, F., Kong, M., & Han, B. (2023). Investigation of the microstructure and properties of CoCrFeNiMo high-entropy alloy coating prepared through high-speed laser cladding. *Coatings, 13*(7), 1211. [CrossRef]

[34] Cui, Y., Shen, J., Manladan, S. M., Geng, K., & Hu, S. (2020). Strengthening mechanism in two-phase FeCoCrNiMnAl high entropy alloy coating. *Applied*

Surface Science, *530*, 147205. [CrossRef]

[35] Sun, S., Wu, Z., Pang, M., Chang, J., Xuan, Y., Qi, H., ... & Wu, Y. (2024). Microstructure and corrosion behavior of chromium-rich stainless steel coatings deposited by different laser cladding processes. *Journal of Materials Research and Technology*, *29*, 3879-3890. [CrossRef]

[36] Meghwal, A., Singh, S., Anupam, A., King, H. J., Schulz, C., Hall, C., ... & Ang, A. S. M. (2022). Nano-and micro-mechanical properties and corrosion performance of a HVOF sprayed AlCoCrFeNi high-entropy alloy coating. *Journal of Alloys and Compounds*, *912*, 165000. [CrossRef]

[37] Meghwal, A., Anupam, A., Luzin, V., Schulz, C., Hall, C., Murty, B. S., ... & Ang, A. S. M. (2021). Multiscale mechanical performance and corrosion behaviour of plasma sprayed AlCoCrFeNi high-entropy alloy coatings. *Journal of Alloys and Compounds*, *854*, 157140. [CrossRef]

[38] Haixiang, C., & Dejun, K. (2020). Comparison on electrochemical corrosion performances of arc and laser thermal sprayed Al–Ti–Ni coatings in marine environment. *Materials Chemistry and Physics*, *251*, 123200. [CrossRef]

[39] Wu, W., & Lin, S. (2024). Wear and corrosion resistances of arc-sprayed FeCr alloy and Fe-based coatings for boiler heat exchanger pipelines. *Journal of Thermal Spray Technology*, *33*(6), 2068-2088. [CrossRef]

[40] Liao, T., Wang, Z., Wu, X., Liu, Q., Guo, Y., Ding, K., & Shang, X. (2023). Effect of V on microstructure, wear and corrosion properties in AlCoCrMoVx high entropy alloy coatings by laser cladding. *Journal of Materials Research and Technology*, *23*, 4420-4431. [CrossRef]

[41] Chen, R., Zheng, C., Ma, H., Yi, G., Ju, D., Zhang, J., ... & Wang, J. (2025). Multi-parameter optimization and corrosion behavior of FeCoNiCrAl HEA coatings via laser cladding. *Metals*, *15*(4), 406. [CrossRef]

[42] Liao, B. K., Liang, Z. X., Luo, Z. G., Liu, Y., Deng, H. W., Zhang, T., ... & Ge, H. E. (2023). Insight into microstructure evolution on anti-corrosion property of Al x CoCrFeNiC0. 01 high-entropy alloys using scanning vibration electrode technique. *Rare Metals*, *42*(10), 3455-3467. [CrossRef]

[43] Bi, D., Chang, Y., Luo, H., Pan, Z., Zhao, Q., Cheng, H., ... & Li, X. (2023). Corrosion behavior and passive film characteristics of AlNbTiZrSix high-entropy alloys in simulated seawater environment. *Corrosion Science*, *224*, 111530. [CrossRef]

Hao Zhang, Male, born in 1992 in Fuyang City, Anhui Province, holds a Doctorate and is an Associate Professor. Research focuses on surface corrosion and protection of light alloys, with a specialisation in the preparation of high-entropy alloy coatings and the investigation of their wear and corrosion protection mechanisms. (Email: zh15695603896@163.com)

Xiujie Yue is affiliated with the Research Institute for Reliability Manufacturing of Intelligent High-End Equipment, Qilu Institute of Technology, Jinan, China. His research focuses on surface and interface engineering of metallic materials and corrosion protection technologies. He investigates advanced surface treatment processes, including water jet surface modification, ultrasonic impact strengthening, and laser shock peening, with particular emphasis on surface microstructure evolution, residual stress distribution, surface roughness, and their effects on material performance. His work aims to reveal the multi-scale coupling mechanisms between surface structures and properties and to improve the mechanical and corrosion resistance of metallic materials under complex service conditions. (Email: yuexiujiea@163.com)

Mengying Qiao, female, born in 1995 in Chifeng City, Inner Mongolia, holds a Master's degree in Chemical Engineering from Inner Mongolia University of Technology. Her research primarily focuses on regulating surface wettability of metals/alloys and designing superhydrophobic functional anti-corrosion coatings. (Email: myqiao0531@163.com)

Miaomiao Xin, born January 1989, Associate Professor, Research Interests: Big Data Technology and Engineering. (Email: mmxin@qlit.edu.cn)